AD-A080 310 WASHINGTON UNIV SEATTLE DEPT OF MECHANICAL ENGINEERING F/G 20/11
DYNAMIC STRESS INTENSITY FACTORS FOR UNSYMMETRIC DYNAMIC ISOCHR--ETC(U)
JAN 80 A S KOBAYASHI, M RAMULU N00014-76-C-0060
UNCLASSIFIED TR-37 NL

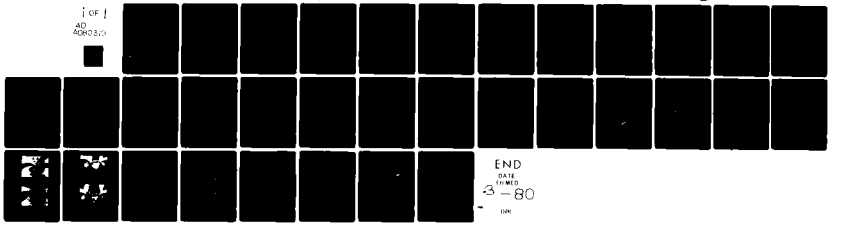

END
DATE FILMED
3-80
DTIC

Office of Naval Research

Contract N00014-76-C-0060 NR 064-478

Technical Report No: 37

DYNAMIC STRESS INTENSITY FACTORS FOR UNSYMMETRIC DYNAMIC ISOCHROMATICS

by

A. S. Kobayashi and M. Ramulu

January 1980

The research reported in this technical report was made possible through support extended to the Department of Mechanical Engineering, University of Washington, by the Office of Naval Research under Contract N00014-76-C-0060 NR 064-478.

Department of Mechanical Engineering
College of Engineering
University of Washington

DYNAMIC STRESS INTENSITY FACTORS FOR UNSYMMETRIC DYNAMIC ISOCHROMATICS

by

A. S. Kobayashi and M. Ramulu

University of Washington
Department of Mechanical Engineering
Seattle, Washington 98195

ABSTRACT

The mixed mode, near-field state of stresses surrounding a crack propagating at constant velocity is used to derive a relation between the dynamic stress intensity factors K_I, K_{II}, the remote stress component σ_{ox} and the dynamic isochromatics. This relation together with an overdeterministic least-square method form the basis of a data reduction procedure for extracting dynamic K_I, K_{II} and σ_{ox} from the recorded dynamic photoelastic pattern surrounding a running crack. The overdeterministic least-square method is also used to fit static isochromatics to the numerically generated dynamic isochromatics. The resultant static K_I, K_{II}, and σ_{ox} are compared with the corresponding dynamic values and estimates of errors involved in using static analysis to process dynamic isochromatic data are obtained. The data reduction procedure is then used to evaluate the branching stress intensity factor associated with crack branching and the mixed mode stress intensity factors associated with crack curving.

INTRODUCTION

In recent years, two dimensional dynamic photoelasticity has been used to determine experimentally the dynamic stress intensity factor surrounding a propagating crack and to establish a dynamic fracture toughness, K_{ID}, versus crack velocity, $\dot{a}$, relation which is believed to control dynamic fracture. An excellent article on this use of dynamic photoelasticity for studying

dynamic fracture has been written recently by J. W. Dally [1]*. Since fracture resistance, i.e. dynamic fracture toughness K_{ID} is equal to the driving force, i.e. instantaneous dynamic stress intensity factor, during crack propagation the dynamic stress intensity factor, which is extracted from transient dynamic isochromatics surrounding the propagating crack tip, is used to measure the dynamic fracture toughness. A commonly used data reduction procedure for this purpose is to fit a theoretical, near-field, static isochromatics to the recorded experimental dynamic isochromatics and to then equate the resultant static stress intensity factor of the former to the unknown dynamic stress intensity factor of the latter [2-5]. Error estimates for using a static near-field stress to extract the dynamic stress intensity factor have been made by several investigators [6-8] and in particular, exhaustively by Rossmanith and Irwin [8].

Studies of the static isochromatic patterns under mixed mode loading conditions, i.e. in the presence of combined K_I and K_{II} crack tip deformation, were made by Smith and Smith [9], Gdousto and Theocaris [10] and more recently by Dally and Sanford [11,12]. These isochromatics are all characterized by their unsymmetric patterns with respect to the crack line. While the simple static isochromatics used to demonstrate the importance of mixed mode loading conditions in the above references were mathematically contrived, Klein determined K_I and K_{II} from actual photoelastic patterns of a crack approaching a hole [13]. Literature, however, is scant on other mixed mode photoelastic investigations despite the well studied theoretical conditions under which such unsymmetric isochromatics can exist.

On the other hand, dynamic isochromatics surrounding a running crack often exhibits moderate unsymmetry but such photoelastic patterns were

*Number in brackets refer to Reference at the end of this paper.

heretofore considered experimental abnormalities and were ignored by averaging the unsymmetric to symmetric patterns during the data reduction process. Careful postmortem inspection of the fracture specimens, however, show that the slightly unsymmetric isochromatics are often associated with slightly curved crack propagation paths which undoubtedly are caused by the small dynamic K_{II}, coexisting with the dominating dynamic K_I value. This effects is akin to the small but noticeable influence of a small K_{II} on fatigue crack propagation reported fifteen years ago [14]. Grossly unsymmetric isochromatics associated with large crack curving, crack branching and propagating multiple cracks, on the other hand, are unmistakably caused by larger K_{II} values. The exact relation between the amount of crack curving and the dynamic K_I and K_{II} associated with the propagating crack tip would provide a dynamic crack propagation law under mixed-mode crack tip deformation similar to the K_{ID} versus å relation under consideration for Mode I dynamic crack propagation [15]. Since the relative magnitude of dynamic K_{II} usually is small with respect to the dynamic K_I values for many crack propagation problems, these K_{II} values must be determined accurately if a meaningful dynamic mixed-mode crack propagation law is to be deduced from these results. The purpose of this investigation is to develop a data reduction procedure for extracting K_I and K_{II} from recorded dynamic isochromatics surrounding a running crack tip. The developed procedure is also used to estimate errors involved in using static mixed-mode crack tip stress field in place of the corresponding dynamic field.

THEORY

The three stress components, σ_{xx}, σ_{yy}, and σ_{xy} in terms of the Modes I and II dynamic stress intensity factors, K_I and K_{II}, plus the remote stress component, σ_{ox},* the maximum shear stress can be represented as [16,17,18]

*Note that the sign conventions of σ_{ox} is negative of that used in References [2,7,8,11,12].

$$\tau_m^2 = \frac{1}{4}\left[H^2 \frac{1}{r} + 2H\cdot\sigma_{ox} \frac{1}{\sqrt{r}} + \sigma_{ox}^2\right] + J^2 \frac{1}{r} \tag{1a}$$

where $H = \frac{K_I}{\sqrt{\pi}} B_I(c) \cdot \left[(1 + s_1^2)\left\{f(c_1) + g(c_1)\right\}^{\frac{1}{2}} - \frac{4s_1s_2}{(1 + s_2^2)}\left\{f(c_2) + g(c_2)\right\}\right]^{\frac{1}{2}}$ (1b)

$$- \frac{K_{II}}{\sqrt{\pi}} B_{II}(c) \cdot \left[(1 + s_1^2)\left\{f(c_1) - g(c_1)\right\}^{\frac{1}{2}} - (1 + s_2^2)\left\{f(c_2) - g(c_2)\right\}^{\frac{1}{2}}\right] \tag{1c}$$

$$J = \frac{K_I}{\sqrt{\pi}} B_I(c) \cdot s_1\left[\left\{f(c_1) - g(c_1)\right\}^{\frac{1}{2}} - \left\{f(c_2) - g(c_2)\right\}^{\frac{1}{2}}\right] \tag{1d}$$

$$+ \frac{K_{II}}{4\sqrt{\pi}\, s_2} B_{II}(c) \cdot \left[4s_1s_2\left\{F(c_1) + g(c_1)\right\}^{\frac{1}{2}} - (1 + s_2^2)^2\left\{f(c_2) + g(c_2)\right\}^{\frac{1}{2}}\right] \tag{1e}$$

$$B_I(c) = \frac{(1 + s_2^2)}{4s_1s_2 - (1 + s_2^2)^2} \tag{1f}$$

$$B_{II}(c) = \frac{2s_2}{4s_1s_2 - (1 + s_2^2)^2} \tag{1g}$$

$$f(c_1) = \frac{1}{\sqrt{1 - \frac{c^2}{c_1^2}\sin^2\theta}} \qquad f(c_2) = \frac{1}{\sqrt{1 - \frac{c^2}{c_2^2}\sin^2\theta}} \tag{1h}$$

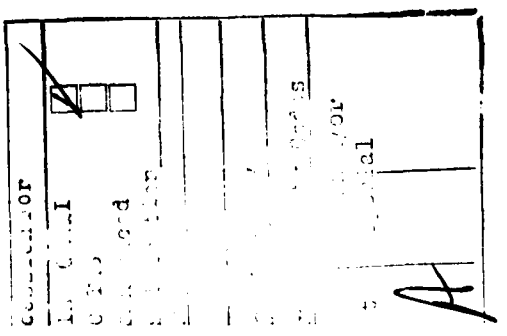

$$g(c_1) = \frac{\cos\theta}{1 - \frac{c^2}{c_1^2}\sin^2\theta} \qquad g(c_2) = \frac{\cos\theta}{1 - \frac{c^2}{c_2^2}\sin^2\theta} \tag{1i}$$

$$s_1^2 = 1 - \frac{c^2}{c_1^2} \qquad s_2^2 = 1 - \frac{c^2}{c_2^2} \tag{1j}$$

r and θ are the traditional polar-coordinates with origin at the moving crack tip and c, c_1, and c_2 are the crack velocity, dilatational and distortional wave velocities, respectively.

For each given θ the radial distance, r, can be explicitly solved from equation (1a) for a given crack velocity, c, mixed mode dynamic stress intensity factors of K_I and K_{II}, and remote stress component of σ_{ox}. Thus the theoretical isochromatics τ_m for a straight crack propagating under constant velocity can be easily constructed. When equation (1) is used to extract K_I and K_{II} from recorded dynamic isochromatics, one can generate 9000 plus isochromatic loops for various combinations of K_I, K_{II}, and σ_{ox} following Etheridge et al. [19] and use a search routine to match the computer stored isochromatics with the experimental isochromatics. In this paper, however, the direct and overdeterministic procedure, which was developed by Bradley [3] and updated with improved numerical techniques by Sanford et al. [12], of least square fitting equation (1) to a large number of measured isochromatic data point is used.

For the above overdeterministic method of least square fitting a theoretical isochromatics τ_m at coordinate locations (r_k, θ_k), equation (1) can be rewritten in a functional form, F_k, which represents the deviation between the square of the calculated and measured isochromatics

$$F_k = \frac{1}{4}\left[H_k^2 \frac{1}{r_k} + 2H_K \sigma_{ox} \frac{1}{\sqrt{r_k}} + \sigma_{ox}^2\right] + J_k^2 \frac{1}{r_k} - \tau_m^2 \tag{2}$$

where k = 1,2,...., is the number of data points on the recorded isochromatic.

Obviously $F_k = 0$ when the theoretical and measured isochromatic coincides. In general, such coincidence cannot be expected and thus K_I, K_{II} and σ_{ox} must be optimized in order to minimize the total summation of F_k. For such minimization, consider:

$$\frac{\partial F_k}{\partial K_I} = \frac{1}{4}\left[2H_k \frac{\partial H_k}{\partial K_I} \frac{1}{r_k} + 2 \frac{\partial H_k}{\partial K_I} \sigma_{ox} \frac{1}{\sqrt{r_k}}\right] + 2J_k \frac{\partial J_k}{\partial K_I} \frac{1}{r_k} \tag{3a}$$

$$\frac{\partial F_k}{\partial K_{II}} = \frac{1}{4}\left[2H_k \frac{\partial H_k}{\partial K_{II}} \frac{1}{r_k} + 2 \frac{\partial H_k}{\partial K_{II}} \sigma_{ox} \frac{1}{\sqrt{r_k}}\right] + 2J_k \frac{\partial J_k}{\partial K_{II}} \frac{1}{r_k} \tag{3b}$$

$$\frac{\partial F_k}{\partial \sigma_{ox}} = \frac{1}{2}\left[H_k \frac{1}{\sqrt{r_k}} + \sigma_{ox}\right] \tag{3c}$$

where $$\frac{\partial H_k}{\partial K_I} = \frac{1}{\sqrt{\pi}} B_I \cdot \left[(1 + s_1^2)\left\{f(c_1) + g(c_1)\right\}^{\frac{1}{2}} - \frac{4s_1 s_2}{(1 + s_2^2}\left\{f(c_2) + g(c_2)\right\}^{\frac{1}{2}}\right] \tag{3d}$$

$$\frac{\partial H_k}{\partial K_{II}} = \frac{-1}{\sqrt{\pi}} B_{II} \cdot \left[(1 + s_1^2)\left\{f(c_1) - g(c_1)\right\}^{\frac{1}{2}} - (1 + s_2^2)\left\{f(c_2) - g(c_2)\right\}^{\frac{1}{2}}\right] \tag{3e}$$

$$\frac{\partial J_k}{\partial K_I} = \frac{1}{\sqrt{\pi}} B_I \cdot s_1 \cdot \left[\left\{f(c_1) - g(c_1)\right\}^{\frac{1}{2}} - \left\{f(c_2) - g(c_2)\right\}^{\frac{1}{2}}\right] \tag{3f}$$

$$\frac{\partial J_k}{\partial K_{II}} = \frac{1}{4\sqrt{\pi}} \frac{B_{II}}{s_2}\left[4s_1 s_2\left\{f(c_1) + g(c_1)\right\}^{\frac{1}{2}} - (1 + s_2^2)^2\left\{f(c_2) + g(c_2)\right\}^{\frac{1}{2}}\right] \tag{3g}$$

The subsequent steps of extracting the optimized K_I, K_{II}, and σ_{ox} using the least square method is a standard numerical procedure which is also identical to that of Reference [12] and thus will not be repeated. Basically, the procedure consists of a sequence of error reduction estimates ΔK_I, ΔK_{II}, and $\Delta\sigma_{ox}$ starting from an initially estimated K_I, K_{II}, and σ_{ox}. The numerical procedure has considered to converge when the current ΔK_I, ΔK_{II}, and $\Delta\sigma_{ox}$ are less than 0.1% of the previously calculated K_I, K_{II} and σ_{ox}.

THEORETICAL ISOCHROMATICS

As one checks on the accuracy of equation (1), the dynamic isochromatics should coincide with that of Reference [11] in the limiting case of crack velocity $c \to 0$. Also informative would be a comparison between this static isochromatics and the corresponding dynamic isochromatics for the identical K_I, K_{II}, and σ_{ox} for a given crack velocity.

In order to provide such theoretical comparison, theoretical isochromatics were generated using the same model fringe constant of f_σ/h = 1.73 MPa/fringe (250 psi/fringe), K_I = .879 MPa $\sqrt{m}$ (800 psi $\sqrt{in}$) and K_{II} of Reference [12]. Static isochromatics were approximated by setting $c = 0.0001\ c_1$ in equation (1). A constant crack velocity of $c = 0.15\ c_1$ was chosen to generate the dynamic isochromatics. In addition c_1 = 2,400 m/sec (94,300 in/sec) and c_2 = 1,160 m/sec (45,800 in/sec) were assumed in the dynamic analysis. In the following some representative static and dynamic isochromatics, which were originally plotted on a CALCOM plotter and then inked for presentation, are shown.

Mode I static and dynamic isochromatics have been studied by others [6,8,20] and thus many of the sample calculations in these references were reproduced as a partial check of the computer code developed for plotting dynamic isochromatics. In particular, the dynamic isochromatics generated in Reference [20] were all reproduced with the new algorithm and the two

results agreed within 0.01 percent. For comparison purpose, some of the results of pure Mode I, pure Mode II and mixed-mode static isochromatics in Reference [12] together with their dynamic counterpart are listed in the following.

Figures 1, 2 and 3 show typical static and dynamic isochromatics of fringe orders, 2.5 and 3.5 surrounding a crack tip. As amply discussed by others [7, 8, 11], for negative values of σ_{ox} the isochromatics lean forward in the direction of crack propagation while for positive values of σ_{ox} the isochromatics lean backward away from the direction of crack propagation. The static isochromatics in Figure 1 coincides with that in Figure 4 of Reference [11]. Figures 2 and 3 show further backwards leaning isochromatics which are due to the higher σ_{ox}/K_I = 0.5 and 0.75. As shown in this figure, the differences between the static and dynamic isochromatics are small for forward leaning loops in Figure 1 but increase slightly with increase in backward leaning angles in Figures 2 and 3.

Figure 4 shows the static and dynamic isochromatics of N = 2.5 and 3.5 for a pure Mode II crack tip deformation. The static results are in agreement with that in Figure 5 of Reference [11]. Unlike the pure Mode I crack tip deformation, little difference between the static and dynamic isochromatics is observed. Experimentally, a crack has seldom been observed to propagate in a straight line under pure Mode II crack tip deformation but will generally curve* to achieve a maximum K_I with attendant smaller K_{II}. Thus a pure Mode II dynamic isochromatic may be a mute academic study. Pure Mode II isochromatics of a stationary crack were reported in Reference [21].

---

*Since the near-field dynamic stress field used to generate the dynamic isochromatics of equation (1a) is for a straight crack, the extent of near-field for a curved crack must be reduced accordingly for this straight crack approximation to hold.

Probably the most frequently encountered mixed-mode static and dynamic isochromatics are generated by the presence of relatively small K_{II} and σ_{ox} coexisting with the K_I mode of crack tip deformation. Figure 5 shows a typical asymmetric isochromatic patterns where some differences between the static and dynamics isochromatics are noted. Figure 6 shows significant change in isochromatic patterns when the sign of the remote stress component σ_{ox} is changed. Needless to say the static isochromatics coincide with those in Figures 8a and 8c, respectively in Reference [11].

Other static isochromatic patterns shown in Reference [11] together with the corresponding dynamic isochromatics were also generated mainly to verify the computer plotted isochromatics for $c = 0.0001\ c_1$ cases. Details of the changes in the shapes of the static isochromatics are discussed thoroughly in Reference [11] and thus will not be reproduced here. In essence the corresponding dynamic isochromatics are found to be slightly larger and essentially follow the general shape of the static isochromatics similar to results shown in Figures 1 through 6.

ERROR ANALYSIS

As mentioned previously, the basic data reduction procedure developed in this investigation consists of least-square-fitting the mixed mode, dynamic near-field state of stress to a large number of data points of a dynamic isochromatic field. For a known constant crack velocity then, this overdeterministic numerical procedure provided the associated dynamic K_I, K_{II}, and σ_{ox}. Internal consistency of this procedure was first verified by least-square fitting a dynamic isochromatic every $\theta_k = 18,36,....,360$, to the theoretical dynamic isochromatic generated for given K_I, K_{II}, and σ_{ox} and then recovering these three dynamic parameters through the overdeterministic method. The recovered K_I, K_{II} and σ_{ox} were within 0.1% of their original values for all five cases represented by Figures 1 through 6.

The differences in static and dynamic isochromatics for the commonly observed maximum crack velocity of about $c = 0.15\ c_1$, as shown in Figures 1 through 6, are relatively small. Nevertheless, a quantitative assessment of the error involved in using static analysis to extract dynamic K_I and K_{II} is necessary since static analysis has been used extensively for reducing the dynamic photoelasticity data associated with a running crack.

Errors involved in using a three-parameter static near-field state of stress to characterize a dynamic isochromatic field associated with a constant velocity crack were estimated by least square fitting a static isochromatics (i.e. $c = 0.0001\ c_1$) to theoretical dynamic isochromatics which were generated through the use of equation (1). The commonly used data reduction procedure was simulated by least square fitting the static field at; 1) three points of θ_{max}* and $\theta_{max} \pm 6°$ along the two dynamic isochromatic lobes on both sides of the crack and 2) along 10 points each straddling θ_{max} and between the maximum width of the two isochromatic lobes on both sides of the arch. The difference between the resultant static K_I, K_{II}, and σ_{ox} and the corresponding dynamic values then constitute the theoretical errors involved in using the static near-field isochromatics for data reduction.

Figure 7 shows the progressive increase in error with increased crack velocity for pure Mode I crack tip deformation. Only the 20 point, i.e. 10 points each on each of the two symmetric isochromatic lobes, data fitting procedure was used for obtaining these results as well as those in Figure 7. Figure 7 shows that errors involved in the overdeterministic method of least-square fitting the near-field static isochromatics of two parameters, K_I and σ_{ox} with $K_{II} = 0$, does not differ substantially with σ_{ox}, with the exception

*For definition of θ_{max}, see References [2,3,5,7,8].

of $\sigma_{ox}/K_I = \pm 0.75$, in the crack velocity range of $c/c_1 < 0.2$ and this finding is in agreement with that of Reference [7]. The lack of systematic changes in errors, i.e. for $\sigma_{ox}/K_I = \pm 0.75$ is an indication that the optimization process involved in the least-square method is functioning properly. Significant, however, is the systematic increase in the error amounting to 13-24 percent of the correct dynamic values at extremely high crack velocity of $c = 0.25\ c_1$. For a crack velocity of $c/c_1 = 0.15$ the estimated errors shown in Figure 7 are within 2∿4 percent of those of Rossmanith and Irwin [8] who conducted a more extensive error analysis involved with Mode I dynamic crack propagation.

In the unlikely event of a dynamic crack propagation under pure Mode II crack tip deformation, a two parameter static stress field, K_{II} and σ_{ox} with $K_I = 0$, can be fitted to this dynamic isochromatics. The errors involved in the fitting process is shown in Figure 8. Unlike the pure Mode I crack tip deformation, the errors involved in using the static near-field stress are small as may have surmised from Figure 4.

Errors estimation in fitting a static near-field mixed mode isochromatic to a mixed-mode dynamic isochromatic will obviously vary with the relative magnitudes of K_I, K_{II} and σ_{ox}. In order to estimate such errors, the static three parameter stress field was least-square fitted to an arbitrary mixed-mode, dynamic isochromatic associated with $K_I = .879$ MPa $\sqrt{m}$ (800 psi $\sqrt{in}$)* and $K_{II} = .219$ MPa $\sqrt{m}$ (200 psi $\sqrt{in}$)* with varying σ_{ox}. Figures 9a and 9b show the widely varying errors in the K_I and K_{II} determined by such optimization procedure. Of particular concern is the unpredicted large errors in K_I and K_{II} associated with higher crack velocities. While this large error could in part be due to the distorted shape of isochromatics as shown in Figure 6,

---

*These values were selected from Reference [11].

these results nevertheless indicate the importance of using the dynamic near field stress for extracting dynamic K_I and K_{II} when the isochromatics are distorted.

EXAMPLES

The developed computer code for computing dynamic K_I, K_{II}, and σ_{ox} was then used to determine the dynamic K_I and K_{II} from the dynamic isochromatics associated with a curving crack and a branching crack.

Figure 10 shows two frames out of a 16-frame dynamic photoelastic record of a curving crack impacting a 12.7 mm (1/2-inch) diameter hole in a 9.53 mm (3/8-inch) thick, 254 x 254 mm (10 x 10 inch) Homalite-100 plate loaded under fixed gripped tension. The crack emanated from a small precrack at the top edge of plate upon reaching a critical load and propagated slightly off the centerline until it was pulled into the higher tension field surrounding the hole. Further details of the experimental stepup, crack velocity measurements and dynamic calibration of the Homalite-100 material used are found in Reference [22].

Figure 11 shows three frames out of a 16-frame dynamic photoelastic record of a crack propagating and branching in a 3.18 mm (1/8-inch) thick, 254 x 254 mm (10 x 10 inch) Homalite-100 plate loaded under fixed-gripped tension. Again details of the experiment can be found in Reference [22].

Figure 12 shows the dynamic K_I and K_{II} variations obtained from the four dynamic photoelastic patterns preceding crack curving and crack impacting the hole as shown in Figure 10. Although not conclusive, the ratio of dynamic K_{II}/K_I increases rapidly prior to crack curving, thus leading to a natural speculation that a moderately mixed mode local dynamic state of stress results in curving of a propagating crack.

Figure 13 shows the dynamic K_I and K_{II} for three branches of the cracks shown in Figure 11. While the continuous "right branch" crack shows moderate changes in dynamic K_I and K_{II}, the left branch shows a sharp drop in dynamic K_I after crack branching. By extrapolating the dynamic K_Is associated with "left branches Nos. 1 and 2", an after-branching dynamic stress intensity factor of 0.923 MPa $\sqrt{m}$ (840 psi $\sqrt{in}$) is obtained. The branching stress intensity factor, i.e. immediately prior to branching, is estimated to be 2.03 MPa $\sqrt{m}$ (1850 psi $\sqrt{in}$). Although this singular data is higher than the branching stress intensity factor of 1.38 MPa $\sqrt{m}$ (1250 psi $\sqrt{in}$) quoted in Reference [1], the ratio of 2.03/0.923 = 2.2 is consistent with the postulate crack branching occurs to dissipate fracture energy along two propagating cracks. It is also interesting to note that dynamic K_{II} which is a relatively low 0.11 MPa $\sqrt{m}$ (100 psi $\sqrt{in}$) prior to crack branching nearly doubles immediately after crack branching and is consistent with the static results of Reference [23].

CONCLUSIONS

1. A data reduction scheme for evaluating the unsymmetric dynamic isochromatic associated with dynamic mixed-mode crack propagation has been developed.

2. Errors involved in using a mixed-mode static near-field stress to evaluate dynamic K_I and K_{II} from a dynamic unsymmetric isochromatics could be larger than that involved for pure Mode I or pure Mode II crack tip deformation.

3. The utility of the developed data reduction procedure was demonstrated.

ACKNOWLEDGEMENT

The results of this investigation were obtained in a research contract funded by the Office of Naval Research under Contract N00014-76-C-0060 NR 064-478. The authors wish to acknowledge the support and encouragement of Dr. N. R. Perrone of ONR during the course of this investigation.

REFERENCES

1. Dally, J. W., "Dynamic Photoelastic Studies of Fracture," Experimental Mechanics, Vol. 19, No. 10, October 1979, pp. 349-367.

2. Irwin, G. R., "Discussion of the Dynamic Stress Distribution Surrounding a Running Crack - A Photoelastic Analysis," Proc. of SESA, Vol. 16, No. 1, 1958, pp. 93-96.

3. Bradley, W. B. and Kobayashi, A. S., "An Investigation of Propagating Crack by Dynamic Photoelasticity," Experimental Mechanics, Vol. 10, No. 3, 1970, pp. 103-113.

4. Bradley, W. B. and Kobayashi, A. S., "Fracture Dynamics - A Photoelastic Investigation," Engineering Fracture Mechanics, Vol. 3, 1971, pp. 317-332.

5. Kobayashi, T. and Dally, J. W., "The Relation Between Crack Velocity and Stress Intensity Factor in Birefringent Polymers," Fast Fracture and Crack Arrest (edited by G. T. Hahn and M. F. Kanninen), ASTM STP 627, 1977, pp. 257-273.

6. Kobayashi, A. S., Wade, B. G., and Bradley, W. B., "Fracture Dynamics of Homalite-100," Deformation and Fracture of High Polymers (edited by H. H. Kausch, J. A. Hassell, and R. I. Jafee), Plenum Press, New York, 1973, pp. 487-500.

7. Irwin, G. R., Dally, J. W., Kobayashi, T., Fourney, W. L., Etheridge, M. J., and Rossmanith, H. P., "On the Determination of the å-K relationships for Birefringent Polymers," Experimental Mechanics, Vol. 19, No. 4, 1979, pp. 121-128.

8. Rossmanith, H. P. and Irwin, G. R., "Analysis of Dynamic Isochromatic Crack-Tip Stress Patterns," University of Maryland Report, 1979.

9. Smith, D. G. and Smith, C. W., "Photoelastic Determination of Mixed Mode Stress Intensity Factors," Engineering Fracture Mechanics, Vol. 4, No. 2, 1972, pp. 357-366.

10. Gdoutos, E. E. and Theocaris, P. S., "A Photoelastic Determination of Mixed-Mode Stress Intensity Factors," Experimental Mechanics, Vol. 18, March 1978, pp. 87-96.

11. Dally, J. W. and Sanford, R. J., "Classification of Stress-Intensity Factors from Isochromatic Fringe Patterns," Experimental Mechanics, Vol. 18, No. 12, Dec. 1978, pp. 441-448.

12. Sanford, R. J. and Dally, J. W., "A General Method for Determining Mixed-Mode Stress Intensity Factors from Isochromatic Fringe Patterns," Engineering Fracture Mechanics, Vol. 11, 1979, pp. 621-633.

13. Klein, G., "Spanningsfaktoren eines Risses in der Umgebung eines Kreisloches und ihr Einfluss auf das Bruchverhalten," Zeitschrift für Werkstofftechnik, Vol. 6, No. 1, 1975, pp. 30-34.

14. Iida, S. and Kobayashi, A. S., "Crack Propagation Rate in 7075-T6 Plates Under Cyclic Tensile and Transverse Shear Loading," J. Of Basic Engineering, Trans. of ASME, Vol. 91, Series D (4), Dec. 1964, pp. 764-769.

15. Dally, J. W., "Dynamic Photoelastic Studies of Fracture," Experimental Mechanics, Vol. 19, No. 10, Oct. 1979, pp. 349-361.

16. Freund, L. B. and Clifton, R. J., "On the Uniqueness of Plane Elastodynamic Solutions for Running Cracks," J. of Elasticity, Vol. 4, No. 4, Dec. 1974, pp. 293-299.

17. Freund, L. B., "Dynamic Crack Propagation," The Mechanics of Fracture, Vol. 19, edited by F. Erdogan, ASME, 1976, pp. 105-134.

18. Freund, L. B., "The Mechanics of Dynamic Shear Crack Propagation," J. of Geophysical Research, Vol. 84, No. 35, 1978, pp. 2199-2209.

19. Etheridge, J. M., Dally, J. W., and Kobayashi, T., "A New Method of Determining the Stress Intensity Factor K from Isochromatic Fringe Loops," Engineering Fracture Mechanics, Vol. 10, No. 1, 1978, pp. 81-93.

20. Kobayashi, A. S. and Mall, S., "Dynamic Fracture Toughness of Homalite-100," Experimental Mechanics, Vol. 18, No. 1, Jan. 1978, pp. 11-18.

21. Kobayashi, A. S., Wade, B. G., Bradley, W. B. and Chiu, S. T., "Crack Branching in Homalite-100 Sheets," Engineering Fracture Mechanics, Vol. 6, 1974, pp. 81-92.

22. Wade, B. G., "A Photoelastic and Numerical Study on Fracture Dynamics of Stressed Panels," Ph.D. thesis submitted to the University of Washington, 1974.

23. Kalthoff, J. F., "On the Propagation Direction of Bifurcated Cracks," Dynamic Crack Propagation (edited by G. C. Sih), Noordhoff International Leyden, 1973, pp. 449-458.

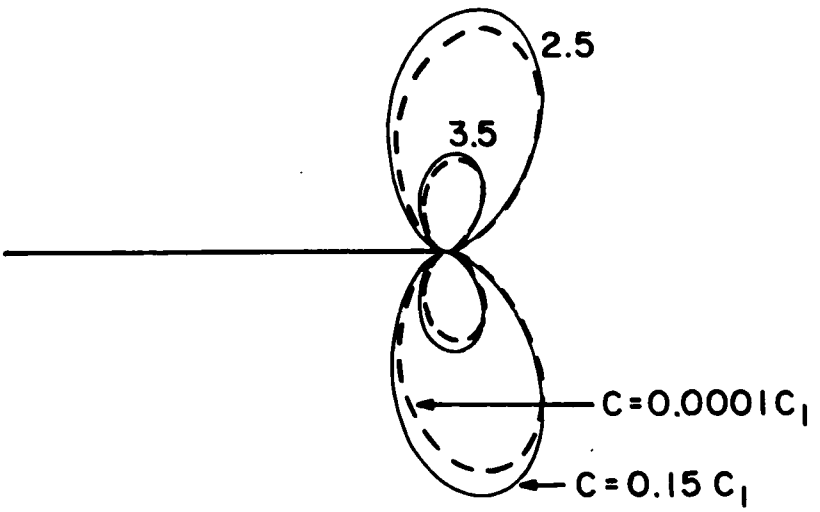

FIGURE 1. STATIC AND DYNAMIC ISOCHROMATICS NEAR A STATIONARY ($C=0.0001\,C_1$) AND PROPAGATING ($C=0.15\,C_1$) CRACK TIP.
$K_I = 800\ \text{psi}\sqrt{\text{in}}$, $K_{II}=0$, $\sigma_{ox} = -0.25\,K_I$ psi

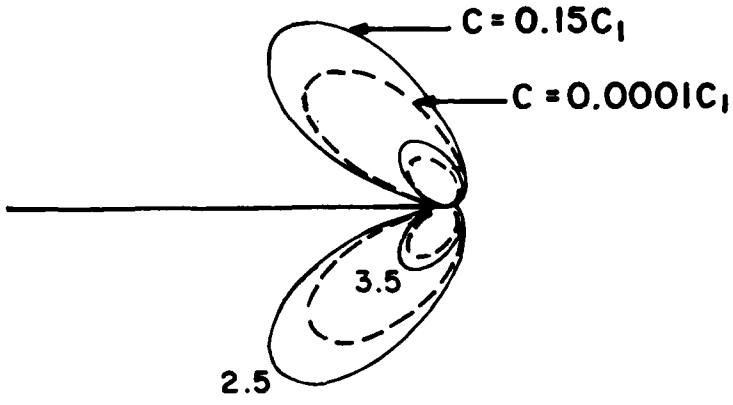

FIGURE 2. STATIC AND DYNAMIC ISOCHROMATICS NEAR A STATIONARY ($C=0.0001C_1$) AND PROPAGATING ($C=0.15C_1$) CRACK TIP.
$K_I = 800 \text{psi}\sqrt{\text{in}}$, $K_{II}=0$, $\sigma_{ox} = 0.5K_I$ psi.

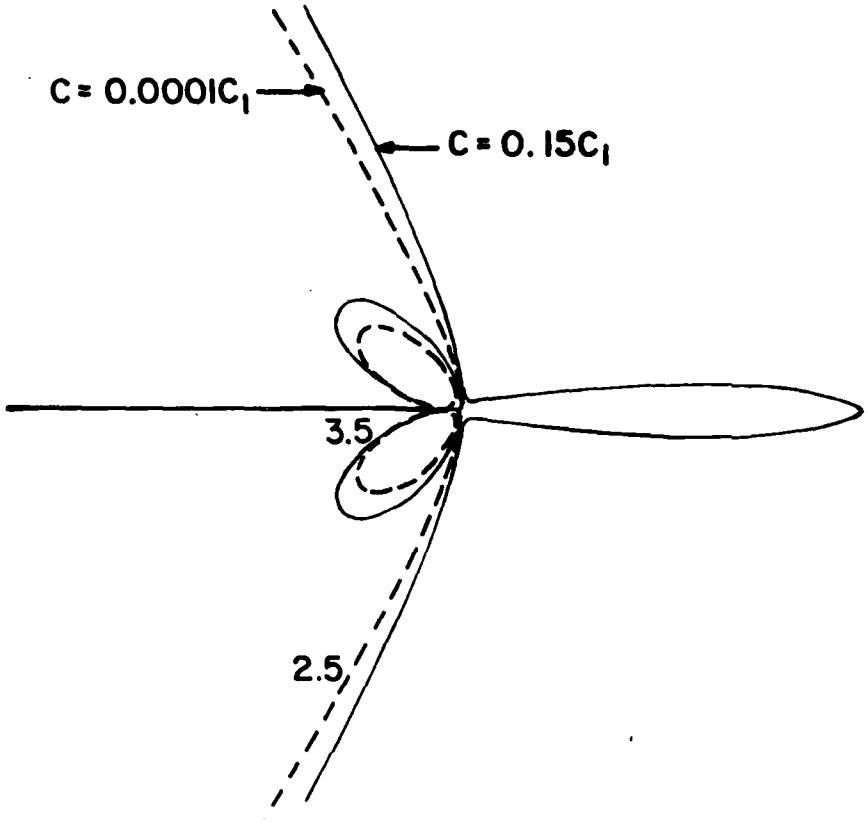

FIGURE 3. STATIC AND DYNAMIC ISOCHROMATICS NEAR A STATIONARY ($C=0.0001C_1$) AND PROPAGATING ($C=0.15C_1$) CRACK TIP.
$K_I = 800$ psi $\sqrt{in}$, $K_{II}=0$, $\sigma_{ox} = 0.75K$ psi.

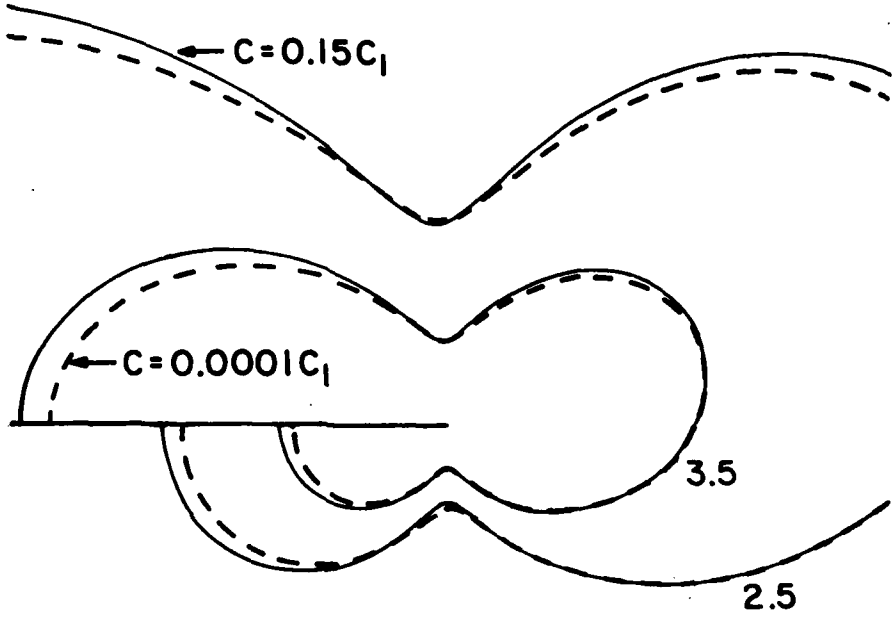

FIGURE 4. STATIC AND DYNAMIC ISOCHROMATICS NEAR A STATIONARY ($C=0.0001C_1$) AND PROPAGATING ($C=0.15C_1$) CRACK TIP.
$K_I=0$, $K_{II}=800 \text{psi}\sqrt{\text{in}}$, $\sigma_{ox}=-0.25K_{II}$ psi

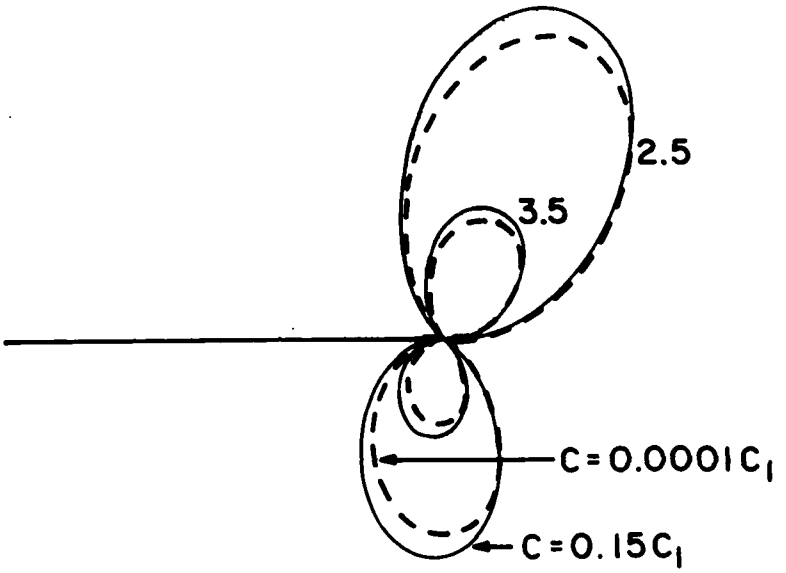

FIGURE 5. STATIC AND DYNAMIC ISOCHROMATICS NEAR A STATIONARY ($C = 0.0001\,C_1$) AND PROPAGATING ($C = 0.15\,C_1$) CRACK TIP.
$K_I = 800\ \text{psi}\sqrt{\text{in}}$, $K_{II} = 0.25\,K_I\ \text{psi}\sqrt{\text{in}}$, $\sigma_{ox} = -0.25\,K_I\ \text{psi}$

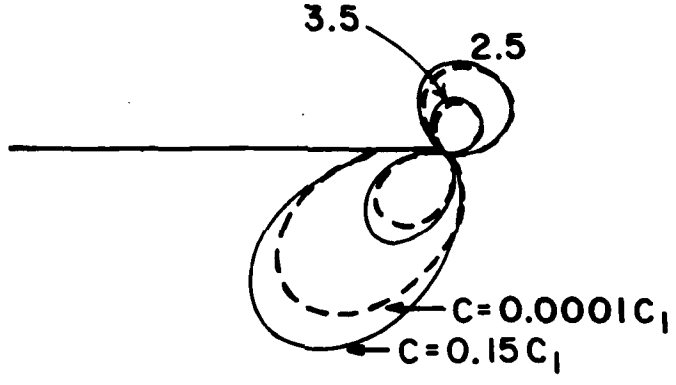

FIGURE 6. STATIC AND DYNAMIC ISOCHROMATICS NEAR A STATIONARY ($C = 0.0001 C_1$) AND PROPAGATING ($C = 0.15 C_1$) CRACK TIP.
$K_I = 800\ \text{psi}\sqrt{\text{in}}$, $K_{II} = 0.25\ K_I\ \text{psi}\sqrt{\text{in}}$, $\sigma_{ox} = -0.25\ K_I\ \text{psi}$

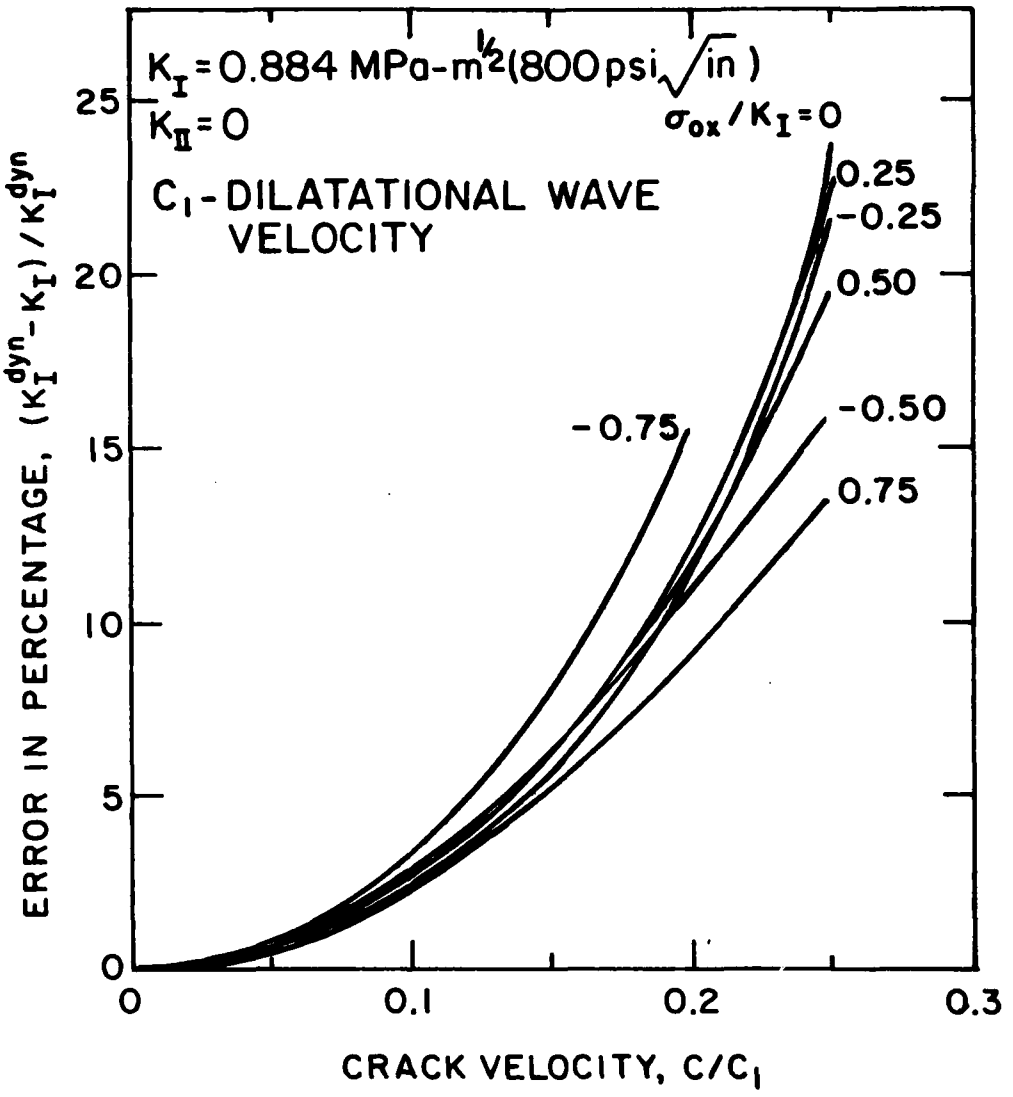

FIGURE 7. ERROR IN DYNAMIC K_I DETERMINATION USING A STATIC TWO-PARAMETER $K_I - \sigma_{ox}$ STRESS FIELD.

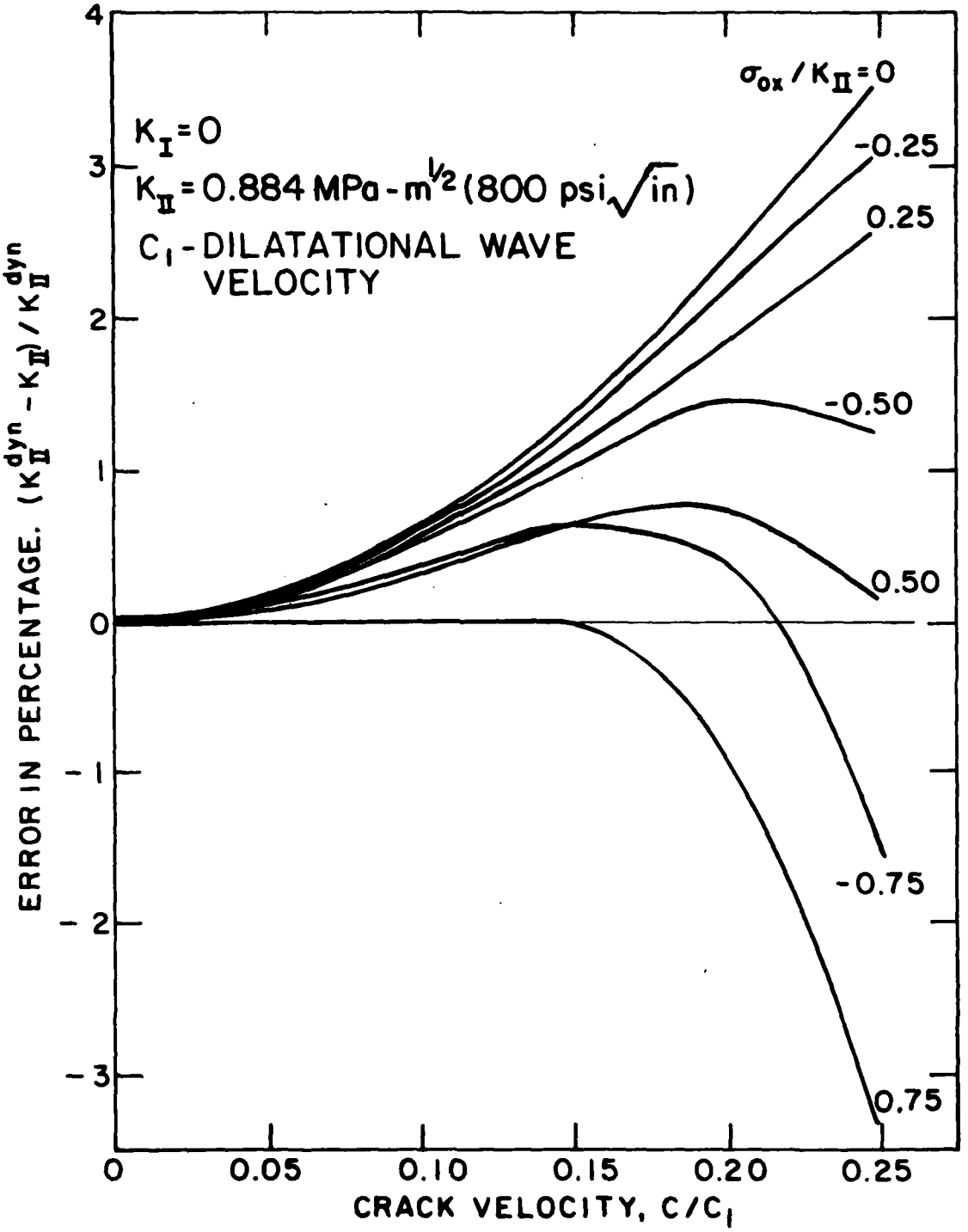

FIGURE 8. ERROR IN DYNAMIC K_{II} DETERMINATION USING A STATIC TWO PARAMETER $K_{II} - \sigma_{ox}$ STRESS FIELD.

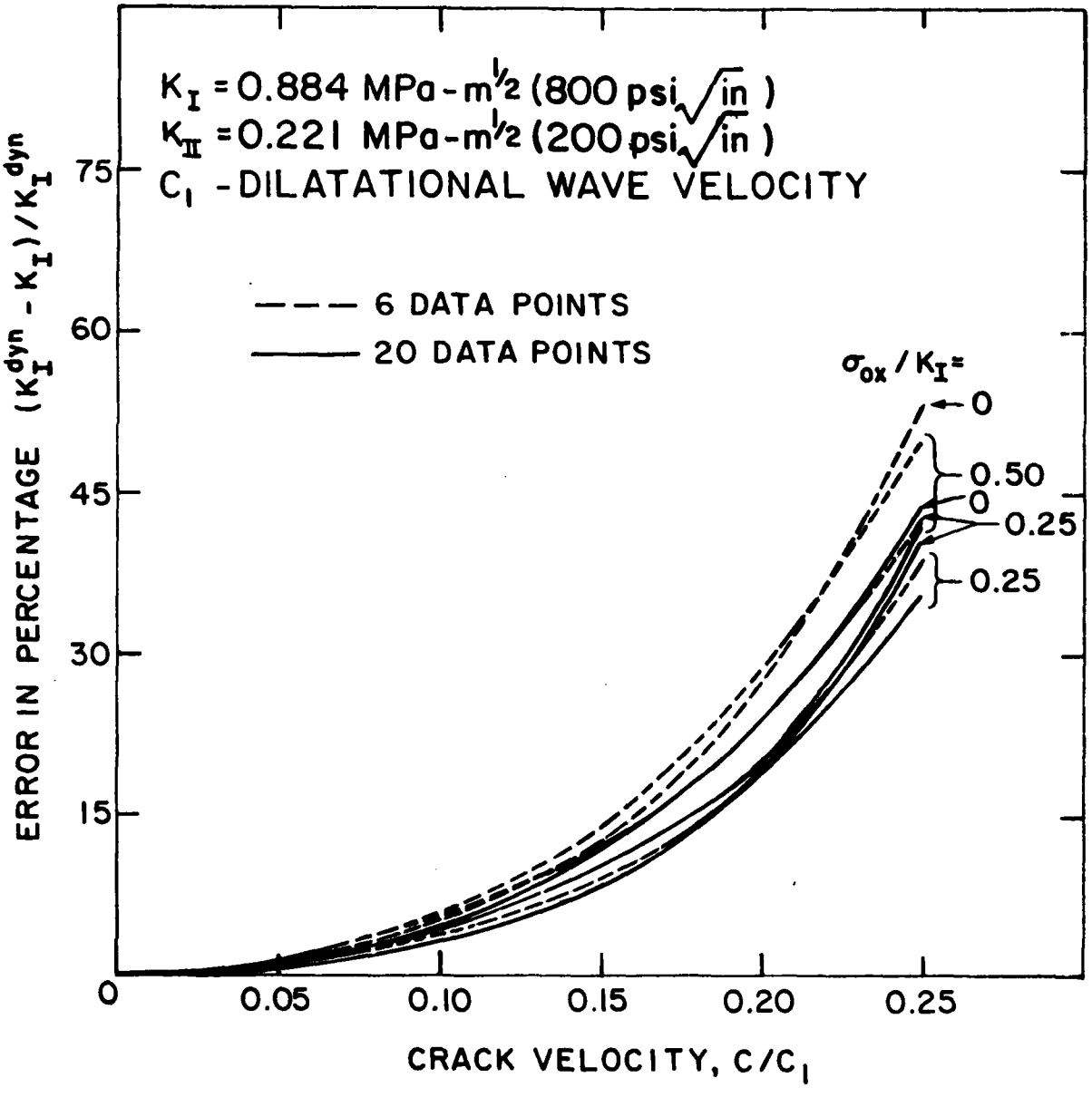

FIGURE 9a. ERRORS IN DYNAMIC K_I DETERMINATION USING A STATIC THREE PARAMETER K_I - K_{II} - σ_{ox} , STRESS FIELD.

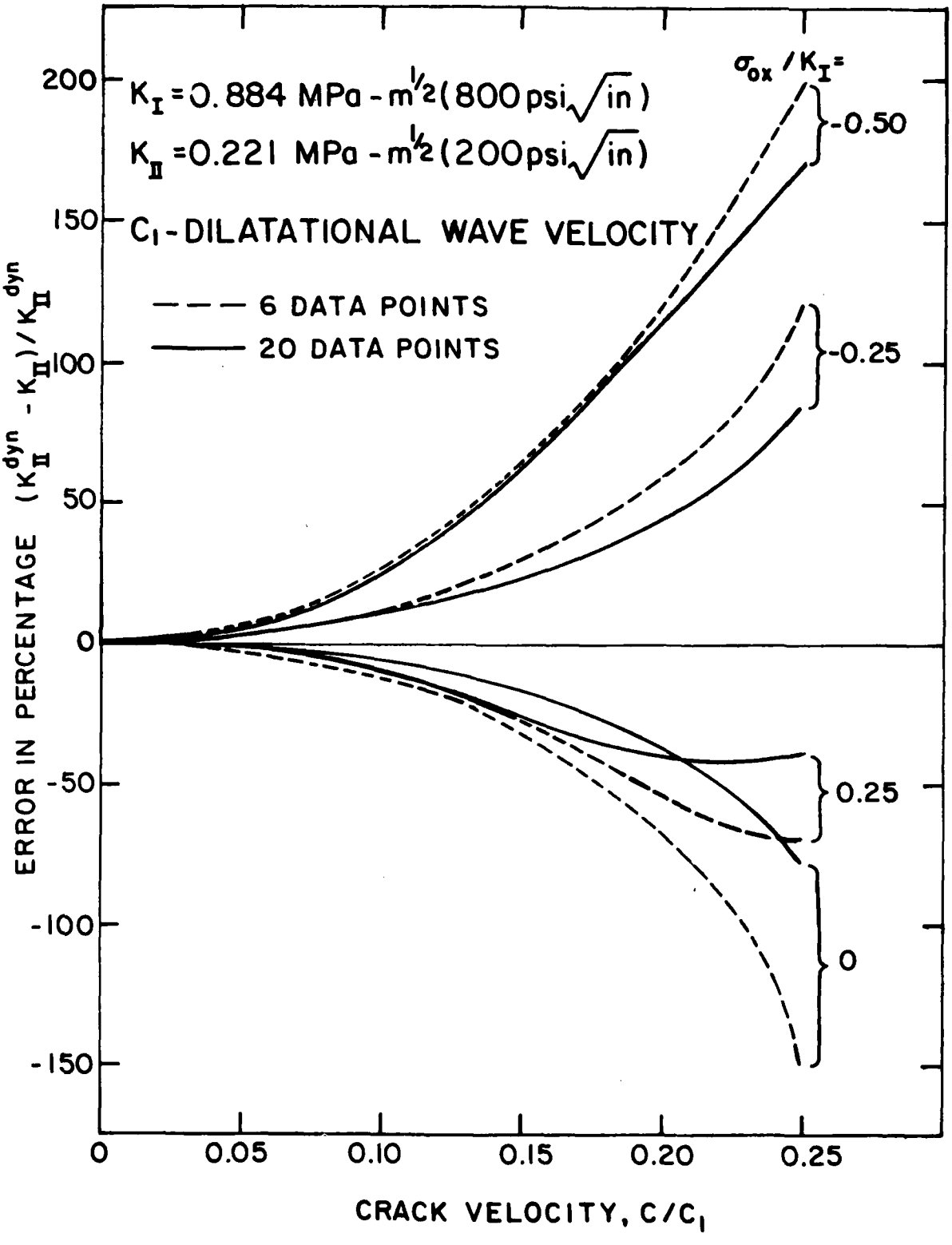

FIGURE 9b . ERRORS IN DYNAMIC K_{II} DETERMINATION USING A STATIC THREE PARAMETER K_I-K_{II}-σ_{ox} ,STRESS FIELD.

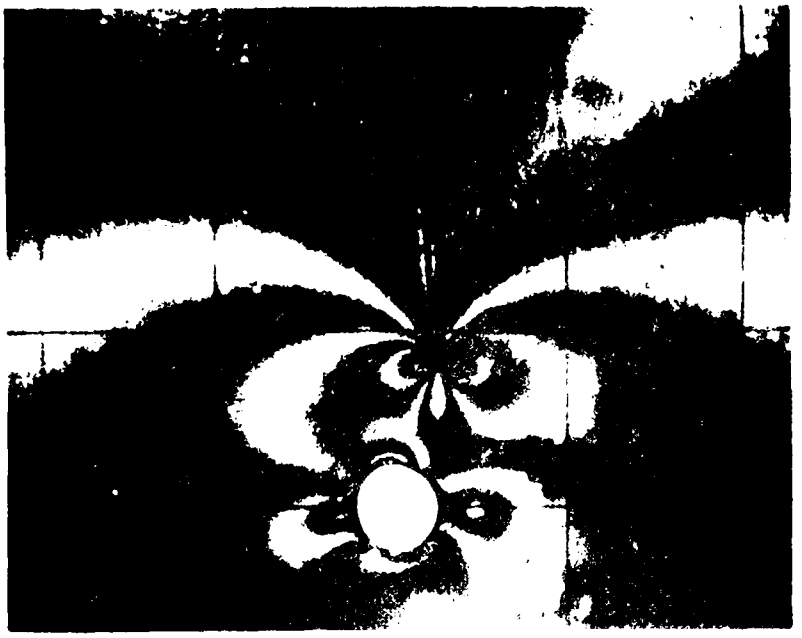

(a) EIGHTH FRAME 175 μ SECONDS

(b) NINETH FRAME 195 μ SECONDS

FIGURE 10. TYPICAL DYNAMIC PHOTOELASTIC PATTERNS IN HOMALITE-100 SINGLE EDGENOTCH SPECIMEN (FIXED GRIP LOADING) CRACK APPROACHING A CENTRAL HOLE, NO. W090220.

(a) EIGHTH FRAME 138 μ SECONDS

(b) ELEVENTH FRAME 225 μ SECONDS

FIGURE 11. TYPICAL CRACK BRANCHING DYNAMIC PHOTOELASTIC PATTERNS IN HOMALITE 100 SINGLE EDGEDNOTCH SPECIMEN (FIXED GRIP LOADING), NO. WO82270.

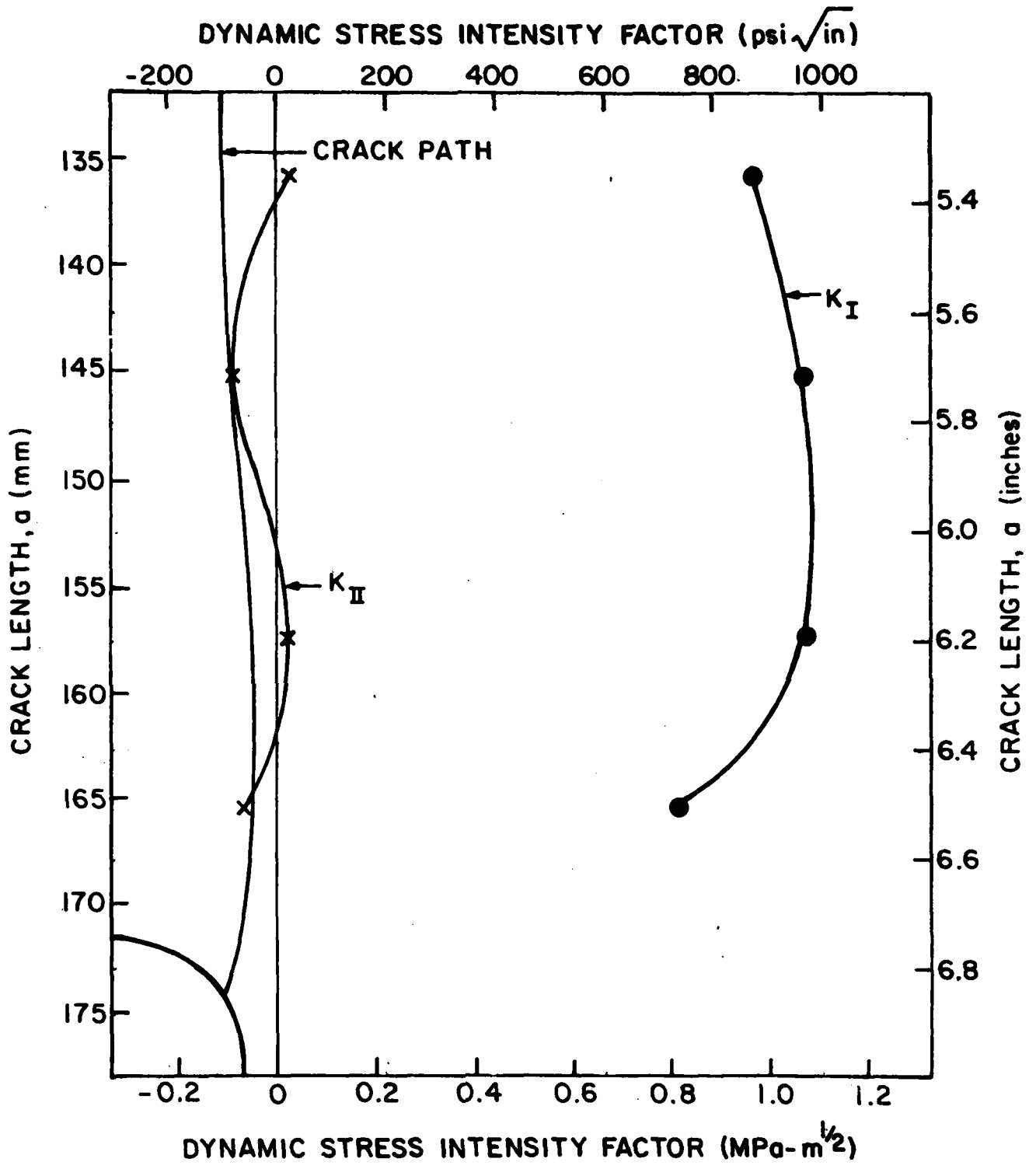

FIGURE 12. DYNAMIC STRESS INTENSITY FACTOR OF CURVED CRACK (FIGURE 10).

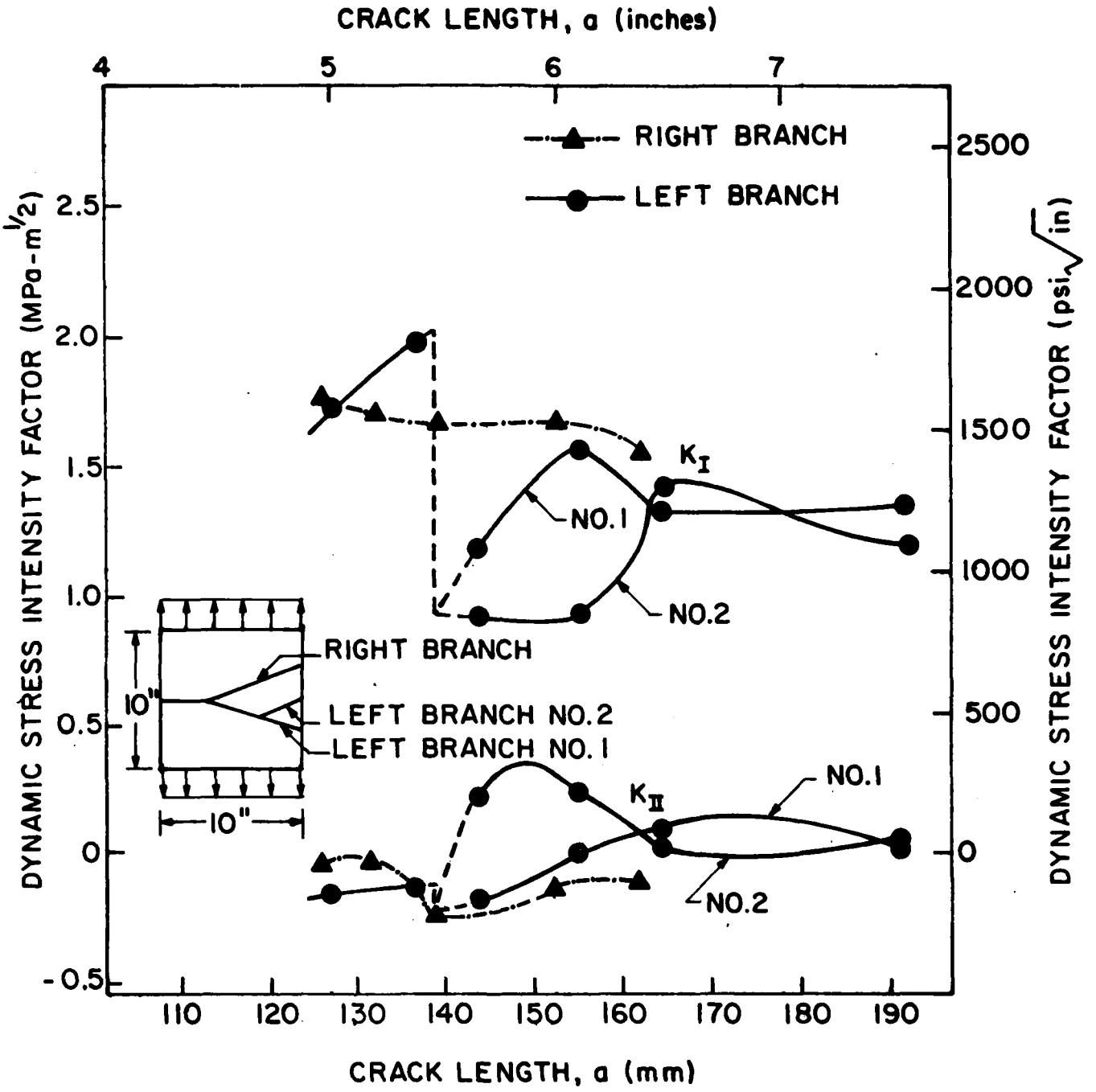

FIGURE 13. DYNAMIC STRESS INTENSITY FACTOR OF A BRANCED CRACK (FIGURE 11.).

Part 1 - Government
Administrative and Liaison Activities

Office of Naval Research
Department of the Navy
Arlington, Virginia 22217
Attn: Code 474 (2)
Code 471
Code 200

Director
Office of Naval Research
Branch Office
666 Summer Street
Boston, Massachusetts 02210

Director
Office of Naval Research
Branch Office
536 South Clark Street
Chicago, Illinois 60605

Director
Office of Naval Research
New York Area Office
715 Broadway - 5th Floor
New York, New York 10003

Director
Office of Naval Research
Branch Office
1030 East Green Street
Pasadena, California 91106

Naval Research Laboratory (6)
Code 2627
Washington, D.C. 20375

Defense Documentation Center (12)
Cameron Station
Alexandria, Virginia 22314

Navy

Undersea Explosion Research Division
Naval Ship Research and Development
Center
Norfolk Naval Shipyard
Portsmouth, Virginia 23709
Attn: Dr. E. Palmer, Code 177

Navy (Con't.)

Naval Research Laboratory
Washington, D.C. 20375
Attn: Code 8400
8410
8430
8440
6300
6390
6380

David W. Taylor Naval Ship Research
and Development Center
Annapolis, Maryland 21402
Attn: Code 2740
28
281

Naval Weapons Center
China Lake, California 93555
Attn: Code 4062
4520

Commanding Officer
Naval Civil Engineering Laboratory
Code L31
Port Hueneme, California 93041

Naval Surface Weapons Center
White Oak
Silver Spring, Maryland 20910
Attn: Code R-10
G-402
K-82

Technical Director
Naval Ocean Systems Center
San Diego, California 92152

Supervisor of Shipbuilding
U.S. Navy
Newport News, Virginia 23607

Navy Underwater Sound
Reference Division
Naval Research Laboratory
P.O. Box 8337
Orlando, Florida 32806

Navy (Con't.)

Chief of Naval Operations
Department of the Navy
Washington, D.C. 20350
Attn: Code OP-098

Strategic Systems Project Office
Department of the Navy
Washington, D.C. 20376
Attn: NSP-200

Naval Air Systems Command
Department of the Navy
Washington, D.C. 20361
Attn: Code 5302 (Aerospace and Structures)
604 (Technical Library)
320R (Structures)

Naval Air Development Center
Warminster, Pennsylvania 18974
Attn: Aerospace Mechanics
Code 606

U.S. Naval Academy
Engineering Department
Annapolis, Maryland 21402

Naval Facilities Engineering Command
200 Stovall Street
Alexandria, Virginia 22332
Attn: Code 03 (Research and Development)
04B
045
14114 (Technical Library)

Naval Sea Systems Command
Department of the Navy
Washington, D.C. 20362
Attn: Code 05H
312
322
323
05R
32R

474:MP:716:Lab
78u474-619

Navy (Con't.)

Commander and Director
David W. Taylor Naval Ship
Research and Development Center
Bethesda, Maryland 20084
Attn: Code 042
17
172
173
174
1800
1844
012.2
1900
1901
1945
1960
1962

Naval Underwater Systems Center
Newport, Rhode Island 02840
Attn: Dr. R. Trainor

Naval Surface Weapons Center
Dahlgren Laboratory
Dahlgren, Virginia 22448
Attn: Code G04
G20

Technical Director
Mare Island Naval Shipyard
Vallejo, California 94592

U.S. Naval Postgraduate School
Library
Code 0384
Monterey, California 93940

Webb Institute of Naval Architecture
Attn: Librarian
Crescent Beach Road, Glen Cove
Long Island, New York 11542

Army

Commanding Officer
U.S. Army Research Office
P.O. Box 12211
Research Triangle Park, NC 27709
Attn: Mr. J. J. Murray, CRD-AA-IP

474:MP:716:Lab
78u474-619

Army (Con't.)

Watervliet Arsenal
MAGGS Research Center
Watervliet, New York 12189
Attn: Director of Research

U.S. Army Materials and Mechanics
Research Center
Watertown, Massachusetts 02172
Attn: Dr. R. Shea, DRXMR-T

U.S. Army Missile Research and
Development Center
Redstone Scientific Information
Center
Chief, Document Section
Redstone Arsenal, Alabama 35809

Army Research and Development
Center
Fort Belvoir, Virginia 22060

NASA

National Aeronautics and Space
Administration
Structures Research Division
Langley Research Center
Langley Station
Hampton, Virginia 23365

National Aeronautics and Space
Administration
Associate Administrator for Advanced
Research and Technology
Washington, D.C. 20546

Air Force

Wright-Patterson Air Force Base
Dayton, Ohio 45433
Attn: AFFDL (FB)
(FBR)
(FBE)
(FBS)
AFML (MBM)

Air Force (Con't.)

Chief Applied Mechanics Group
U.S. Air Force Institute of Technology
Wright-Patterson Air Force Base
Dayton, Ohio 45433

Chief, Civil Engineering Branch
WLRC, Research Division
Air Force Weapons Laboratory
Kirtland Air Force Base
Albuquerque, New Mexico 87117

Air Force Office of Scientific Research
Bolling Air Force Base
Washington, D.C. 20332
Attn: Mechanics Division

Department of the Air Force
Air University Library
Maxwell Air Force Base
Montgomery, Alabama 36112

Other Government Activities

Commandant
Chief, Testing and Development Division
U.S. Coast Guard
1300 E Street, NW.
Washington, D.C. 20226

Technical Director
Marine Corps Development
and Education Command
Quantico, Virginia 22134

Director Defense Research
and Engineering
Technical Library
Room 3C128
The Pentagon
Washington, D.C. 20301

474:MP:716:Lab
78u474-619

Other Government Activities (Con't)

Dr. M. Gaus
National Science Foundation
Environmental Research Division
Washington, D.C. 20550

Library of Congress
Science and Technology Division
Washington, D.C. 20540

Director
Defense Nuclear Agency
Washington, D.C. 20305
Attn: SPSS

Mr. Jerome Persh
Staff Specialist for Materials
and Structures
OUSDR&E, The Pentagon
Room 3D1089
Washington, D.C. 20301

Chief, Airframe and Equipment Branch
FB-120
Office of Flight Standards
Federal Aviation Agency
Washington, D.C. 20553

National Academy of Sciences
National Research Council
Ship Hull Research Committee
2101 Constitution Avenue
Washington, D.C. 20418
Attn: Mr. A. R. Lytle

National Science Foundation
Engineering Mechanics Section
Division of Engineering
Washington, D.C. 20550

Picatinny Arsenal
Plastics Technical Evaluation Center
Attn: Technical Information Section
Dover, New Jersey 07801

Maritime Administration
Office of Maritime Technology
14th and Constitution Avenue, NW.
Washington, D.C. 20230

474:MP:716:Lab
78u474-619

PART 2 - Contractors and Other Technical Collaborators

Universities

Dr. J. Tinsley Oden
University of Texas at Austin
345 Engineering Science Building
Austin, Texas 78712

Professor Julius Miklowitz
California Institute of Technology
Division of Engineering
and Applied Sciences
Pasadena, California 91109

Dr. Harold Liebowitz, Dean
School of Engineering and
Applied Science
George Washington University
Washington, D.C. 20052

Professor Eli Sternberg
California Institute of Technology
Division of Engineering and
Applied Sciences
Pasadena, California 91109

Professor Paul M. Naghdi
University of California
Department of Mechanical Engineering
Berkeley, California 94720

Professor A. J. Durelli
Oakland University
School of Engineering
Rochester, Missouri 48063

Professor P. L. DiMaggio
Columbia University
Department of Civil Engineering
New York, New York 10027

Professor Norman Jones
The University of Liverpool
Department of Mechanical Engineering
P. O. Box 147
Brownlow Hill
Liverpool L69 3BX
England

Professor E. J. Skudrzyk
Pennsylvania State University
Applied Research Laboratory
Department of Physics
State College, Pennsylvania 16801

Universities (Con't.)

Professor J. Klosner
Polytechnic Institute of New York
Department of Mechanical and
Aerospace Engineering
333 Jay Street
Brooklyn, New York 11201

Professor R. A. Schapery
Texas A&M University
Department of Civil Engineering
College Station, Texas 77843

Professor Walter D. Pilkey
University of Virginia
Research Laboratories for the
Engineering Sciences and
Applied Sciences
Charlottesville, Virginia 22901

Professor K. D. Willmert
Clarkson College of Technology
Department of Mechanical Engineering
Potsdam, New York 13676

Dr. Walter E. Haisler
Texas A&M University
Aerospace Engineering Department
College Station, Texas 77843

Dr. Hussein A. Kamel
University of Arizona
Department of Aerospace and
Mechanical Engineering
Tucson, Arizona 85721

Dr. S. J. Fenves
Carnegie-Mellon University
Department of Civil Engineering
Schenley Park
Pittsburgh, Pennsylvania 15213

Dr. Ronald L. Huston
Department of Engineering Analysis
University of Cincinnati
Cincinnati, Ohio 45221

Universities (Con't)

Professor G. C. M. Sih
Lehigh University
Institute of Fracture and
Solid Mechanics
Bethlehem, Pennsylvania 18015

Professor Albert S. Kobayashi
University of Washington
Department of Mechanical Engineering
Seattle, Washington 98105

Professor Daniel Frederick
Virginia Polytechnic Institute and
State University
Department of Engineering Mechanics
Blacksburg, Virginia 24061

Professor A. C. Eringen
Princeton University
Department of Aerospace and
Mechanical Sciences
Princeton, New Jersey 08540

Professor E. H. Lee
Stanford University
Division of Engineering Mechanics
Stanford, California 94305

Professor Albert I. King
Wayne State University
Biomechanics Research Center
Detroit, Michigan 48202

Dr. V. R. Hodgson
Wayne State University
School of Medicine
Detroit, Michigan 48202

Dean B. A. Boley
Northwestern University
Department of Civil Engineering
Evanston, Illinois 60201

Universities (Con't)

Professor P. G. Hodge, Jr.
University of Minnesota
Department of Aerospace Engineering
and Mechanics
Minneapolis, Minnesota 55455

Dr. D. C. Drucker
University of Illinois
Dean of Engineering
Urbana, Illinois 61801

Professor N. M. Newmark
University of Illinois
Department of Civil Engineering
Urbana, Illinois 61803

Professor E. Reissner
University of California, San Diego
Department of Applied Mechanics
La Jolla, California 92037

Professor William A. Nash
University of Massachusetts
Department of Mechanics and
Aerospace Engineering
Amherst, Massachusetts 01002

Professor G. Herrmann
Stanford University
Department of Applied Mechanics
Stanford, California 94305

Professor J. D. Achenbach
Northwest University
Department of Civil Engineering
Evanston, Illinois 60201

Professor S. B. Dong
University of California
Department of Mechanics
Los Angeles, California 90024

Professor Burt Paul
University of Pennsylvania
Towne School of Civil and
Mechanical Engineering
Philadelphia, Pennsylvania 19104

Universities (Con't)

Professor H. W. Liu
Syracuse University
Department of Chemical Engineering
and Metallurgy
Syracuse, New York 13210

Professor S. Bodner
Technion R&D Foundation
Haifa, Israel

Professor Werner Goldsmith
University of California
Department of Mechanical Engineering
Berkeley, California 94720

Professor R. S. Rivlin
Lehigh University
Center for the Application
of Mathematics
Bethlehem, Pennsylvania 18015

Professor F. A. Cozzarelli
State University of New York at
Buffalo
Division of Interdisciplinary Studies
Karr Parker Engineering Building
Chemistry Road
Buffalo, New York 14214

Professor Joseph L. Rose
Drexel University
Department of Mechanical Engineering
and Mechanics
Philadelphia, Pennsylvania 19104

Professor B. K. Donaldson
University of Maryland
Aerospace Engineering Department
College Park, Maryland 20742

Professor Joseph A. Clark
Catholic University of America
Department of Mechanical Engineering
Washington, D.C. 20064

Universities (Con't)

Dr. Samuel B. Batdorf
University of California
School of Engineering
and Applied Science
Los Angeles, California 90024

Professor Isaac Fried
Boston University
Department of Mathematics
Boston, Massachusetts 02215

Professor E. Krempl
Rensselaer Polytechnic Institute
Division of Engineering
Engineering Mechanics
Troy, New York 12181

Dr. Jack R. Vinson
University of Delaware
Department of Mechanical and Aerospace
Engineering and the Center for
Composite Materials
Newark, Delaware 19711

Dr. J. Duffy
Brown University
Division of Engineering
Providence, Rhode Island 02912

Dr. J. L. Swedlow
Carnegie-Mellon University
Department of Mechanical Engineering
Pittsburgh, Pennsylvania 15213

Dr. V. K. Varadan
Ohio State University Research Foundation
Department of Engineering Mechanics
Columbus, Ohio 43210

Dr. Z. Mashin
University of Pennsylvania
Department of Metallurgy and
Materials Science
College of Engineering and
Applied Science
Philadelphia, Pennsylvania 19104

Universities (Con't)

Dr. Jackson C. S. Yang
University of Maryland
Department of Mechanical Engineering
College Park, Maryland 20742

Professor T. Y. Chang
University of Akron
Department of Civil Engineering
Akron, Ohio 44325

Professor Charles W. Bert
University of Oklahoma
School of Aerospace, Mechanical,
and Nuclear Engineering
Norman, Oklahoma 73019

Professor Satya N. Atluri
Georgia Institute of Technology
School of Engineering and
Mechanics
Atlanta, Georgia 30332

Professor Graham F. Carey
University of Texas at Austin
Department of Aerospace Engineering
and Engineering Mechanics
Austin, Texas 78712

Dr. S. S. Wang
University of Illinois
Department of Theoretical and
Applied Mechanics
Urbana, Illinois 61801

Industry and Research Institutes

Dr. Norman Hobbs
Kaman AviDyne
Division of Kaman
Sciences Corporation
Burlington, Massachusetts 01803

Argonne National Laboratory
Library Services Department
9700 South Cass Avenue
Argonne, Illinois 60440

Industry and Research Institutes (Con't)

Dr. M. C. Junger
Cambridge Acoustical Associates
54 Rindge Avenue Extension
Cambridge, Massachusetts 02140

Dr. V. Godino
General Dynamics Corporation
Electric Boat Division
Groton, Connecticut 06340

Dr. J. E. Greenspon
J. G. Engineering Research Associates
3831 Menlo Drive
Baltimore, Maryland 21215

Newport News Shipbuilding and
Dry Dock Company
Library
Newport News, Virginia 23607

Dr. W. F. Bozich
McDonnell Douglas Corporation
5301 Bolsa Avenue
Huntington Beach, California 92647

Dr. H. N. Abramson
Southwest Research Institute
8500 Culebra Road
San Antonio, Texas 78284

Dr. R. C. DeHart
Southwest Research Institute
8500 Culebra Road
San Antonio, Texas 78284

Dr. M. L. Baron
Weidlinger Associates
110 East 59th Street
New York, New York 10022

Dr. T. L. Geers
Lockheed Missiles and Space Company
3251 Hanover Street
Palo Alto, California 94304

Mr. William Caywood
Applied Physics Laboratory
Johns Hopkins Road
Laurel, Maryland 20810

Industry and Research Institutes (Con't)

Dr. Robert E. Dunham
Pacifics Technology
P.O. Box 148
Del Mar, California 92014

Dr. M. F. Kanninen
Battelle Columbus Laboratories
505 King Avenue
Columbus, Ohio 43201

Dr. A. A. Hochrein
Daedalean Associates, Inc.
Springlake Research Road
15110 Frederick Road
Woodbine, Maryland 21797

Dr. James W. Jones
Swanson Service Corporation
P.O. Box 5415
Huntington Beach, California 92646

Dr. Robert E. Nickell
Applied Science and Technology
3344 North Torrey Pines Court
Suite 220
La Jolla, California 92037

Dr. Kevin Thomas
Westinghouse Electric Corp.
Advanced Reactors Division
P. O. Box 158
Madison, Pennsylvania 15663

Unclassified

SECURITY CLASSIFICATION OF THIS PAGE (When Data Entered)

REPORT DOCUMENTATION PAGE

READ INSTRUCTIONS BEFORE COMPLETING FORM

1. REPORT NUMBER: TR 35	2. GOVT ACCESSION NO.
3. RECIPIENT'S CATALOG NUMBER	
4. TITLE (and Subtitle): Dynamic Stress Intensity Factors for Unsymmetric Dynamic Isochromatics,	5. TYPE OF REPORT & PERIOD COVERED: Technical Report,
6. PERFORMING ORG. REPORT NUMBER: TR-37	
7. AUTHOR(s): A. S. Kobayashi [redacted] M. Ramulu	8. CONTRACT OR GRANT NUMBER(s): N00014-76-C-0060
9. PERFORMING ORGANIZATION NAME AND ADDRESS: Dept. of Mechanical Engineering FU-10, University of Washington, Seattle, WA 98195	10. PROGRAM ELEMENT, PROJECT, TASK AREA & WORK UNIT NUMBERS: NR 064-478
11. CONTROLLING OFFICE NAME AND ADDRESS: Office of Naval Research, Arlington, Virginia 22217	12. REPORT DATE: Jan [redacted] 80
	13. NUMBER OF PAGES: 28
14. MONITORING AGENCY NAME & ADDRESS (if different from Controlling Office)	15. SECURITY CLASS. (of this report): Unclassified
	15a. DECLASSIFICATION/DOWNGRADING SCHEDULE

16. DISTRIBUTION STATEMENT (of this Report)

Unlimited

DISTRIBUTION STATEMENT A
Approved for public release;
Distribution Unlimited

17. DISTRIBUTION STATEMENT (of the abstract entered in Block 20, if different from Report)

18. SUPPLEMENTARY NOTES

19. KEY WORDS (Continue on reverse side if necessary and identify by block number)
Dynamic stress intensity factors, dynamic fracture mechanics, dynamic finite element analysis, dynamic photoelasticity

20. ABSTRACT (Continue on reverse side if necessary and identify by block number)
The mixed mode, near-field state of stresses surrounding a crack propagating at constant velocity is used to derive a relation between the dynamic stress intensity factors K_I, K_{II}, the remote stress component σ_{ox} and the dynamic isochromatics. This relation together with an overdeterministic least-square method form the basis of a data reduction procedure for → next page

DD FORM 1 JAN 73 1473 EDITION OF 1 NOV 65 IS OBSOLETE
S/N 0102-014-6601

Unclassified
SECURITY CLASSIFICATION OF THIS PAGE (When Data Entered)

extracting dynamic K_I, K_{II} and σ_{ox} from the recorded dynamic photoelastic pattern surrounding a running crack. The overdeterministic least-square method is also used to fit static isochromatics to the numerically generated dynamic isochromatics. The resultant static K_I, K_{II}, and σ_{ox} are compared with the corresponding dynamic values and estimates of errors involved in using static analysis to process dynamic isochromatic data are obtained. The data reduction procedure is then used to evaluate the branching stress intensity factor associated with crack branching and the mixed mode stress intensity factors associated with crack curving.

K sub I, K sub II, and sigma sub OX